Jurnal Kejuruteraan 35(6) 2023: 1311-1327
https://doi.org/10.17576/jkukm-2023-35(6)-05

Wing Planform Analysis with Taper Ratio and Expansion Segment Variation with Lifting Line Theory

Amien S. Dafa* & Gunawan Nugroho

Department of Engineering Physics, Institut Teknologi Sepuluh Nopember
Kampus ITS Sukolilo, Surabaya Indonesia 60111

**Corresponding author: asd12amien@gmail.com; gunawan@ep.its.ac.id*

Received 6 October 2022, Received in revised form 5 April 2023
Accepted 5 May 2023, Available 30 November 2023

ABSTRACT

Tapered wing shape of a planform wing is still widely used amongst airplane and UAVs with subsonic speed. In the design process, a good consideration for a good taper ratio of a wing is required to obtain the optimal and distribution for the desired function of an aircraft. Additionally, addition of expansion segment on wing planform shape is often used to increase the performance of wings without the increase of wingspan. Several methods to analyze a wing shape are experimentation, computational luid dynamics, and analytical calculation. Analyzing with analytical calculation will present limited, but accurate outcomes due to the assumptions that are made during the calculation. This method, however, is inexpensive. This is why analytical calculation is still a common method to use in the design process of an aircraft, particularly in the early phase. Five variants of taper ratio and 3 variants that with expansion segment is analyzed using the Lifting Line Theory that utilizes Fourier series at subsonic speed. The results are the values of and with respect to and the distribution of and along the wingspan. Increasing the taper ratio results in the decrease of and the increase of , while adding an expansion segment will give results that are dependent on the added segment's taper ratio.

Keywords: Lifting Line Theory; taper ratio; expansion segment

INTRODUCTION

Aviation industries have grown far from where it began in the early 20th century. Early aircrafts were biplane aircrafts, which have a pair of wings, while recent aircrafts have more wing shape variations. Since its discovery, functionality of aircrafts has also grown. Aircrafts who could only fly for 30 kmph to 40 kmph can now fly in the supersonic region, which is above 1234.8 kmph. The most important part of an aircraft is the wing. Parameters such as wing area, wing planform shape, airfoil shape, wingspan, angle of incident, and wingtip affect the characteristic and performances of an aircraft. Several research had been done to increase the efficiency of aircrafts through innovations on wings, both on the planform shape and the airfoil shape. The wing planform shape parameter can affect the vortex distribution that generates lift and *induced drag* that is also generated by the consequences of finite wing (John D. Anderson, 2011). One way to consider those parameters are with lift coefficient and induced drag that can be calculated with Lifting Line Theory.

Despite being an old method, Lifting Line Theory is still widely used in 3-dimensional wing analysis because of the simplicity and accuracy that it provides. Lifting Line Theory (LLT) was used to calculate lift distribution on wings that flaps and twist that mimic bird wings were researched to obtain maneuverability control (Jacob S. Izraelevitz, 2017). It was used to create a model to calculate and analyze 3-dimensional rotary wings (Luis A. Martinez-Tossas, 2019). There are several other methods besides LLT that can be use to analyze a 3-dimensional wing, such as LES (Large Eddy Simulation) which used grid and several grid size variations was analyzed to find the optimal grid size used for that method (Kengo Asada, 2018), and IDDES (Delayed Detached Eddy Simulation). Other researches regarding wing planform shape was also done to analyze the effects of wing planform shape, such as

(Tyler Van Buren, 2017)that found concave trailing edge shape increases thrust and efficiency of a wing, leading edge tubercles were found to increase lift generated by a wing and postpone stall (Ming Zhao, 2017), but only on several phase and wavelength of tubercles (Michael D. Bolzon., 2016), and motions of the wing, such as heaving and pitching on foils that affect the efficiency of a wing (Daniel Floryan, 2017).

As mentioned earlier, there are several other methods besides LLT that can be used to analyze a 3-dimensional wings, such as Computational Fluid Dynamics (CFD), such LES or IDDES and Experimentation, which are both very accurate, but also very expensive and consume a considerable amount of time, whereas the former being inferior in all aspects than the latter. This reason is why analytical calculations such as Surface Line Method, Vortex Lattice Method, and Lifting Line Theory is still widely used because those methods are straightforward, very inexpensive, and quite accurate. Lifting Line Theory analyticsl calculation provides life coefficient per unit span distribution and induced drag coefficient per unit span distribution from a wing planform shape with a modest cost that can be used as a preliminary analysis in the early phase of aircraft design.

The importance of wing planform shape, one of the parameter of a wing can be seen in several aircrafts, such as ATR-72, Pilatus PC-21, and Cessna-172 that have tapered planform wing shape (Yildirim, 2021) and fly at the subsonic region, Airbus A3 series and Boeing 737 and 747 series that have a swept back wing planform shape and fly at the transonic region, and supersonic aircrafts, such as Concord, AV-8B Harier, and Falcon Fighter series that have a delta wing planform shape. Despite having reached the supersonic speed, modern medium sized commercial aircrafts focuses fly at subsonic and transonic region, due to several reasons (Johnson, 1990)- (Slotnick, 2019). Aircrafts with designed for each speed region have different functionalities. Commercial flights for short-medium range do not need transonic speed as it will be redundant. Short-medium range flights utilizes subsonic aircrafts, which uses tapered wing planform shape. Tapered wing shapes already provide good performances for a wing, but engineers try to increase its performances by adding an expansion segment with the idea of increasing its wing area without increasing the wingspan. These are due to several consequences of increasing wingspan, such as airport infrastructures, aircrafts own inertia, and structural consideration (Kermode, 2006). This article will calculate and analyze several wing planform shapes with Lifting Line Theory for the early phase design of a small-medium sized low-medium speed aircraft, particularly in the subsonic speed (0.185 Mach to 0.434 Mach).

THEORITICAL FRAMEWORK

MASS CONSERVATION AND CONTINUITY

Cited from (Yunus A. Cengel, 2014), when observing fluids, there are 2 major obersvation methods, Lagrangian and Eulerian. Lagrangian obervation observes a particle and follows it along its path, while Eulerian observations observes fluids with a ”window” and observes all the particles that flow through that ”window”. The latter is commonly used in fluid mechanics and both hydrodynamics and aerodynamics. This is due to the observation of fluid object or fluid body such as wings, automotives, and turbines. If an assumption is given with a Eularian observation, such that a flow is 1 direction (x direction), the common equation that is used in continuity is:

$$\frac{\partial(\rho u)}{\partial x}+\frac{\partial(\rho v)}{\partial y}+\frac{\partial(\rho w)}{\partial z}=-\frac{\partial \rho}{\partial t} \tag{1}$$

Where ρ is the fluid dens*ity, u,v* and are the velocity component on *x, y*, and *z* directions respectively. Another assumption, incompressible flow can change (1) to:

$$\frac{\partial u}{\partial x}+\frac{\partial v}{\partial y}+\frac{\partial w}{\partial z}=0 \tag{2}$$

Other form of conservation equation is the conservation of momentum:

$$\rho\left(\frac{\partial u}{\partial t}+\frac{u\partial u}{\partial x}+\frac{v\partial u}{\partial y}+\frac{w\partial u}{\partial z}\right)=-\frac{\partial p}{\partial x}+\mu\left(\frac{\partial^2 u}{\partial x^2}+\frac{\partial^2 u}{\partial y^2}+\frac{\partial^2 u}{\partial z^2}\right)+\rho g \tag{3}$$

Where the left hand side of the equation is the acceleration (traditional and convective) and on the right hand side of the equation are the normal force (pressure), tangential force (viscosity) μ and its couple, and body forces (currently gravity, but can also be magnetic and other forces). If (3) is given assumptions, such as steady, inviscid, 1-dimensional flow, no body forces, and flow along streamline, (3) will become:

$$\begin{gathered}\rho u\frac{\partial u}{\partial x}=-\frac{dp}{dx}\\ \rho u\partial u=-dp\\ \int \rho u\partial u=\int -dp\\ \frac{1}{2}\rho u^2=-P+constant\\ p+\frac{1}{2}\rho u^2=constant\end{gathered} \tag{4}$$

Which is the Bernoulli equation. This is the informal derivation of the Bernoulli equation, as the formal derivation is too extensive to be written here.

LAPLACE EQUATION

Cited from (John D. Anderson, 2011) and (Edward Lewis Houghton, 2013), Laplace equation states that a del squared of a function f(x,y,z) equals to zero. Del squared ∇^2 is also called laplace operator.

$$\nabla^2 f=0 \tag{5}$$

If laplace from a equation equals to zero, that equation satisfies the laplace equation. This equation is very well-known in physics and maths as it describes electromagnetism, heat energy, and fluids. In fluids, there are two specific equations that satisfy the laplace equation, which are velocity potential $(f = \phi)$ and stream function $(f = \psi)$. Both equations satisfy the laplace equation particularly with several assumptions, such as inviscid, incompressible, and irrotational. The definition of velocity potential comes from equating the velocity components to their corresponding spatial gradient of the potential.

$$u = \frac{\partial \phi}{\partial x}, v = \frac{\partial \phi}{\partial y}, w = \frac{\partial \phi}{\partial z} \tag{6}$$

Where (6) can be substituted to (2) to obtain:

$$\frac{\partial^2 \phi}{\partial x^2} + \frac{\partial^2 \phi}{\partial y^2} + \frac{\partial^2 \phi}{\partial z^2} = 0 \tag{7}$$

Where (7) satisfies the laplace equation $(\nabla^2 \phi=0)$. Meanwhile, stream function is the velocity set equal to the opposite spatial derivative of the scalar function.

$$u = \frac{\partial \psi}{\partial y}, v = -\frac{\partial \psi}{\partial x} \tag{8}$$

Both equations on (8) is related by the irrotational assumption, which is defined by:

$$\frac{\partial v}{\partial x} - \frac{\partial u}{\partial y} = 0 \tag{9}$$

If (8) is substituted to (9), the laplace equation can be satisfied.

$$-\frac{\partial^2 \psi}{\partial x^2} - \frac{\partial^2 \psi}{\partial y^2} = 0 \tag{10}$$

(7) and (10) justify that both velocity potential and stream function satisfy the laplace equation, particularly with assumptions that were mentioned earlier. Therefore, these equations can only be used in a flow that is incompressible and is boundary layers.

GENERAL LIFT DISTRIBUTION

Cited from (John D. Anderson, 2011) and (Edward Lewis Houghton, 2013), the vortex distribution of elliptical wing is:

$$\Gamma(z) = \Gamma_0 \sqrt{1 - \left(\frac{2y}{b}\right)^2} \tag{11}$$

Where Γ_0 is vortex in the position. Vortex size varies along the span, but (11) only defines the vortex distribution on a specific condition, where the wing is unaffected by anything. Therefore, generalization of the vortex distribution is needed. This is possible by substituting $y = -\frac{b}{2}\cos\theta$ to convert the coordinates from Cartesians to Cylindrical coordinates with a span of $0 \leq \theta \leq \pi$. Hence, (11) will be converted to:

$$\Gamma(\theta) = \Gamma_0 \sin\theta \tag{12}$$

(12) informs that Fourier series can be used to obtain the general vortex distribution along the span. Therefore, (12) is possible to be converted to:

$$\Gamma(\theta) = 2bV \sum_{n=1}^{N} A_n \sin n\theta \tag{13}$$

Where *N* in the equation is the number of calculation iteration that can be changed to determine the preferred accuracy on the calculation, while A_n $(n=1,2,\ldots,N)$ is unknown but must satisfy the Lifting Line Theory equation in (22) and (23).

PRANDTL'S LIFTING LINE THEORY

Commonly, wing analysis are done on the 2-dimensional airfoil. This is invalid as real wings are 3-dimensional and finite. This finite wing has a side effect called downwash that is generated at the tip of the wing. Downwash generates vortices that produce drag and reduce effective lift that is produced by the wing (John D. Anderson, 2011).

Cited from (John D. Anderson, 2011) and (Edward Lewis Houghton, 2013), Lifting Line Theory is a method to predict and calculate lift coefficient per unit span C_l, overall lift coefficient , induced drag coefficient per unit

span , and overall induced drag coefficient on a finite wing. This is an old but accurate method that is still commonly used nowadays due to its simplicity and accuracy. The results however are limited due to the several assumptions that is required to use this method such as incompressible, inviscid, and irrotational. This method combines the Biot-Savart Law for the downwash velocity equation and the Kutta-Jokowski theorem to relate vortex with lift. One segment of horseshoe vortex with cartesian coordinates along the span *z*, can be defined by:

$$dw = -\frac{\left(\frac{d\Gamma}{dz}\right)dz}{4\pi(z_o - z)} \tag{14}$$

and horseshoe vortex for one wing, which is the integral of (14) to the number of segments that is calculated can be defined by

$$w = -\frac{1}{4\pi}\int_{-b/2}^{b/2}\frac{\left(\frac{d\Gamma}{dz}\right)}{z - z_1}dz \tag{15}$$

Where *w* is the downwash and (15) defines the downwash that is produced by Γ that is still unknown. While on ideal condition, lift coefficient increases along with angle of attack (Zuhairi A. Rashid, 2021), this is not the case as downwash reduce the effective angle of attack for the lift generation. (15) can be used to calculate the induced angle of attack ε, which is the decrease of effective angle of attack due to downwash. If a small angle assumption is given $\left(\varepsilon = \tan^{-1}\left(-\frac{w}{V}\right) \approx \left(-\frac{w}{V}\right)\right)$, induced angle of attack can be defined by:

$$\varepsilon = -\frac{1}{4\pi u_\infty}\int_{-b/2}^{b/2}\frac{\left(\frac{d\Gamma}{dz}\right)}{4\pi(z_o - z)}dz \tag{16}$$

Where the induced angle of attack becomes a vortex function. The relation between induced angle of attack and effective angle of attack that was mentioned earlier is:

$$\alpha_\infty = \alpha - \varepsilon \tag{17}$$

Where α_∞ is the effective angle of attack, is the angle of attack, and ε is the effective angle of attack. With the thin airfoil theory, lift slope can be calculated without the consideration of airfoil camber:

$$\begin{gathered}\frac{dC_L}{d\alpha} = 2\pi = a_\infty \\ dC_L = 2\pi\, d\alpha \\ C_L = 2\pi(\alpha_\infty - \alpha_0) = a_\infty(\alpha_\infty - \alpha_0)\end{gathered} \tag{18}$$

Where is the angle of attack offset due to the cambered airfoil, commonly known, is the 2-dimensional slope of the airfoil and mostly equal to . However, if both airfoil on the root and tip of the wing differs, needs to be interpolated by the data of each airfoil. If (17) is substituted to (18), the following equation can be obtained:

$$C_L = a_\infty[(\alpha - \alpha_0) - \varepsilon] \tag{19}$$

And from the Kutta-Joukowski theorem, lift per unit span can be calculated with the vortex Γ

$$l = \frac{1}{2}\rho V^2 c C_L = \rho V \Gamma \tag{20}$$

Equation (20) can be arranged to

$$C_l = \frac{2\Gamma}{a_\infty c} = V[(\alpha - \alpha_0) - \varepsilon] \tag{21}$$

Its already known that by the small angle assumption that were mentioned earlier. Subsequently, (15) can be substituted to (21) to obtain

$$\frac{2\Gamma}{a_\infty c} = V(\alpha - \alpha_0) + \frac{1}{4\pi}\int_{-b/2}^{b/2}\frac{\left(\frac{d\Gamma}{dz}\right)}{z - z_1}dz = V(\alpha - \alpha_0) - w \tag{22}$$

Where (22) is the general solution for the Lifting Line Theory for every vortex along the span. Equation (22) can further be simplified by subtituting (13) to (22) to obtain

$$w = \frac{V\sum_{n=1}^{N} A_n \sin n\theta}{\sin\theta}$$

Which can be substituted to (22) to obtain

$$2\frac{2bV\sum_{n=1}^{N} A_n \sin n\theta}{a_\infty c} = V(\alpha - \alpha_0) - \frac{V\sum_{n=1}^{N} A_n \sin n\theta}{\sin\theta}$$

Where *V* can be crossed out. If a notation is given, such that $ca_\infty/4b$ is equal to μ , the equation above will become

$$\mu(\alpha - \alpha_0) = \sum_{n=1}^{N} A_n \sin n\theta\left(1 + \frac{\mu n}{\sin\theta}\right) \tag{23}$$

To calculate with (13), the span coordinates must be converted to cylindrical coordinates from cartesian, with a transformation of:

$$z = -\frac{b\cos\theta}{2} \tag{24}$$

Results from the calculation of (23) will be in the form of constants A_n ($A_1, A_2, \ldots, A_n$), which are still yet to be known with a number of constants that were predetermined. Those constants will further be calculated to obtain Γ, which will then be used to obtain

a) Lift per unit span from the Kutta-Joukowski theorem

$$l = l(\theta) = \rho V \Gamma(\theta) \tag{25}$$

Lift coefficient per unit span with (21) and overall lift coefficient

$$C_L = A_1 \pi (AR) \tag{26}$$

Which can be used to find lift force

$$\mathrm{L} = \frac{1}{2} C_L \rho V^2 S \tag{27}$$

Induced drag per unit span

$$d_v = d_v(\theta) = \rho w \Gamma(\theta) = \mathrm{l}\varepsilon \tag{28}$$

Where (28) can be used to find the induced drag coefficient per unit span

$$\mathrm{C}_{\mathrm{d}_v} = \frac{dv}{\frac{1}{2}\rho V^2 c} \tag{29}$$

And the overall induced drag coefficient

$$\mathrm{C}_{\mathrm{D}_v} = \frac{C_L^2}{\pi (AR)} \tag{30}$$

Where (30) can be used to find induced drag force

$$\mathrm{D_v} = \frac{1}{2} C_{D_v} \rho V^2 S \tag{31}$$

Where *AR* and *S* will be explained afterwards.

ASPECT RATIO

Aspect ratio (*AR*) is a non-dimensional number that represents the narrowness of a wing [4] and [13]. Aspect ratio is defined by

$$AR = \frac{b^2}{S} \tag{32}$$

Where *b* is the length of wingspan and *S* the area of the wing planform shape. Rectangular wing, however, has a different equation for aspect ratio, which is defined by $AR = b/S$. *AR* affects several parameters of wings, such as

b) Induced angle of attack

$$\varepsilon = \frac{kC_L}{\pi (AR)} \tag{33}$$

Where kC_L is the total drag coefficient that depends on lift (also known as C_{D_L} [13]).

a) Lift coefficient that is written in (26)

b) Induced drag coefficient that is written in (30)

1. NACA Airfoil

NACA airfoil is a type of airfoil that is developed by NACA (National Advisory Committee for Aeronautics), where there are 3 series that were developed, which are 4-digit series, 5-digit series, and 6-digit series. In NACA 4-digit series (which is used in this research), the first digit represents the maximum camber in hundredths of chord, the second digit represents the maximum camber location in tenths of chord measured from the leading edge, and the last 2 digits represent the maximum thickness of the airfoil in hundredths of chord. Chord itself is a straight line that passes the leading edge and the trailing edge of the airfoil, while camber is a line where every points in it has the same distance to the upper and lower surface of the airfoil.

CALCULATION METHOD

CALCULATION PROCEDURES

To obtain the and with Lifting Line Theory, the calculation must be done by

1. Obtaining wing variables needed to input in the calculation, such as *b,z,θ,S,λ,AR,* and *N*.
2. Obtaining fluids variables such as *Re,V∞* or *V* , and *ρ* to obtain the 2D airfoil data that are used in the calculation.
3. Obtaining 2-dimensional airfoil variables in the mid-span and the tip of the wing, such as α, a_{∞}, and α_0.
4. Initialization (in support calculation program) for several variables, such as α^o, ε, α_{eff}, and α_{∞}.
5. For the segmentation of the wings (in calculation), coordinates are needed to identify the calculation location according to wingspan. Therefore, z for Cartesian coordinates dan θ for Cylindrical coordinates are used. Interpolation is used to identify each location and iteration, which is defined by $X = DMS\left[1 - \frac{DMS-DWT}{DMS}\left(\frac{z}{s}\right)\right]$, for variables such as α (for wings with geometric twist), a_{∞} dan α_0 (for wings with airfoil morph or different airfoils along the span), and c.
6. Calculation is done with (23) that is modified into

$$\alpha^o = A_n\left(\frac{\sin n\theta}{\mu} + \frac{n \sin n\theta}{\sin\theta}\right)$$

where $\left(\frac{\sin n\theta}{\mu} + \frac{n \sin n\theta}{\sin\theta}\right)$ noted as F, and the equation becomes

$$\alpha^o = A_n \times F$$
$$A_n = \alpha^o \times F^{-1}$$

Which will provides data in the form of A_n matrix that can be used to calculate Γ with (13)

7. matrix that has been obtained is then used to calculate C_l, C_{d_v}, C_L, C_{D_v}, l, L, d_v, D_v and ε with (21), (29), (26), (30), (25), (27), (28), (31), dan (33) respectively.

$$C_l = \frac{2\Gamma}{cV_{\infty}}$$
$$C_{d_v} = \frac{d_v}{\frac{1}{2}\rho_{air}V_{\infty}^2 c}$$
$$C_L = \pi A_1 (AR)$$
$$C_{D_v} = \pi(AR)\Sigma n A_n^2$$
$$l = \rho_{air}V_{\infty}\Gamma$$
$$L = \frac{1}{2}C_L\rho_{air}V_{\infty}^2 S$$
$$d_v = \rho_{air}w\Gamma = l\varepsilon$$
$$D_v = \frac{1}{2}C_{D_v}\rho_{air}V_{\infty}^2 S$$
$$\varepsilon = \frac{\Sigma n A_n \sin n\theta}{\sin\theta}$$

8. After all results has been obtained, the results are then plotted into graphs.

VALIDATION

Validation of the calculation is done by comparing the result of one variant to [Justin Petrilli, 2013] with the same fluid variables, which are airfoil data from Reynolds numbers of , air density of for altitude [Engineering Toolbox, 2003], and freestream velocity of . The wing variables of this variant are , wing taper ratio, and NACA 4415 airfoil. The wings that are calculated here are symmetrical, all the Figures only represent half of the wing. As for taper ratio , is defined by , with is the chord length on the tip of the wing is the chord length in the middle of the wing.

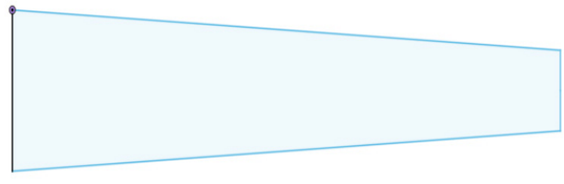

FIGURE 1. Validation variant with AR = 12 and λ = 0.5 [14].

TAPER RATIO VARIANT

There are 5 variants that are used to vary different taper ratio of a wing. The fluid variables that are used are the same with the validation variables. Each variant has an increase in *taper ratio* from A-TR to E-TR sequentially with an interval of . All 5 variants use the same airfoil, which is NACA 2312.

1. A-TR Variant with λ = 1/3 and AR = 6.

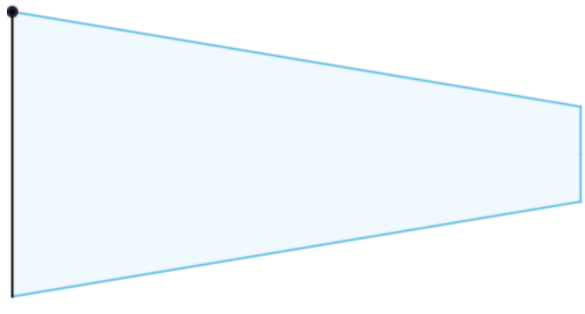

FIGURE 2. A-TR variant with λ = 1/3 and AR = 6.

2. B-TR Variant with λ = 1/2 and *AR = 16/3*.

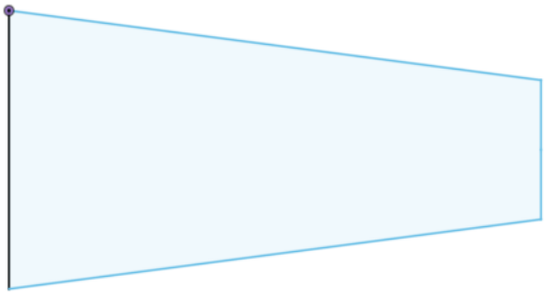

FIGURE 3. B-TR variant λ = 1/2 and *AR = 16/3*.

3. C-TR Variant with λ = 2/3 and *AR = 4.8*.

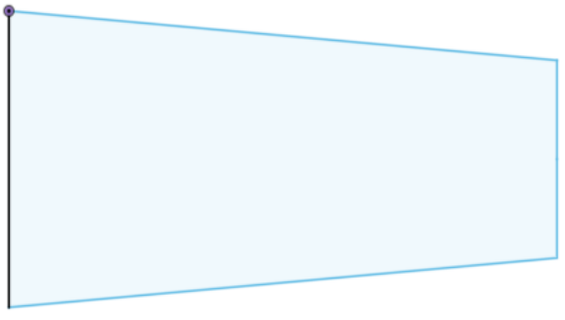

FIGURE 4. C-TR variant with λ = 2/3 and *AR = 4.8*.

4. D-TR Variant with λ = 5/6 and AR = 48/11.

FIGURE 5. D-TR variant with λ = 5/6 and AR = 48/11.

5. E-TR Variant with λ = 1 and AR = 4.

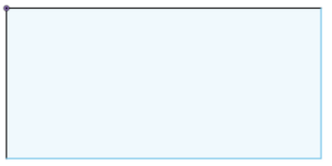

FIGURE 6. E-TR variant with λ = 1 and AR = 4.

EXPANSION SEGMENT VARIANT

There are 3 variants that are used to analyze the effect of adding an expansion segment on a wing planform shape. Fluid variables are the same with the validation variables. All 3 variants use the same airfoil, which is NACA 2312.

1. A-S Variant without expansion segment with λ = 1/2 and *AR = 52/9*.

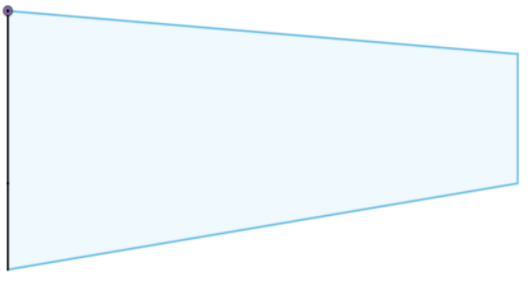

FIGURE 7. A-S variant with λ = 1/2 and *AR = 52/9*.

2. B-S Variant with an expansion segment of λ = 5/6 and and *AR = 5/11* and total AR_{total}*=679/119*.

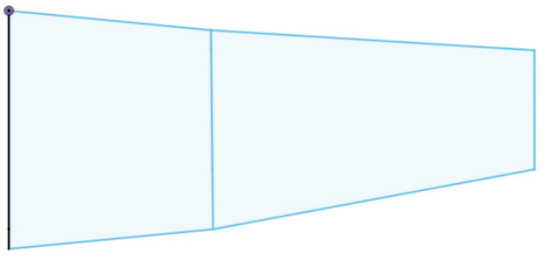

FIGURE 8. A-S variant with an expansion segment of λ = 5/6 and AR = 5/11 and total AR_{total}*=679/119*.

3. C-S Variant with an expansion segment of λ = 1 and AR = 5/12 and total AR_{total}=*169/33*.

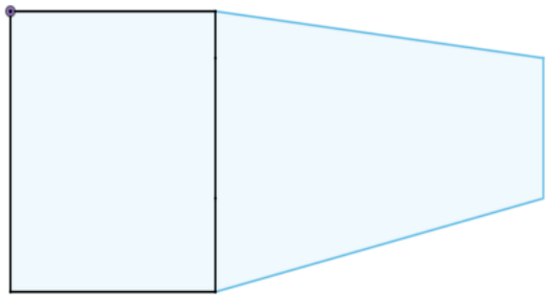

FIGURE 9. A-S variant with an expansion segment of λ = 1 and AR = 5/12 and total AR_{total}=*169/33*.

RESULTS AND DISCUSSION

1. Validation Results

Validation is done by comparing data obtained from the Lifting Line Theory analytical calculation to [14]. C_L obtained from the calculation seems to concur with the C_L from [14] up to , which can be seen in Figure 10. Figure 10 also shows corellation between and . The distribution of and is also shown in Figure 11 with 3 different , where

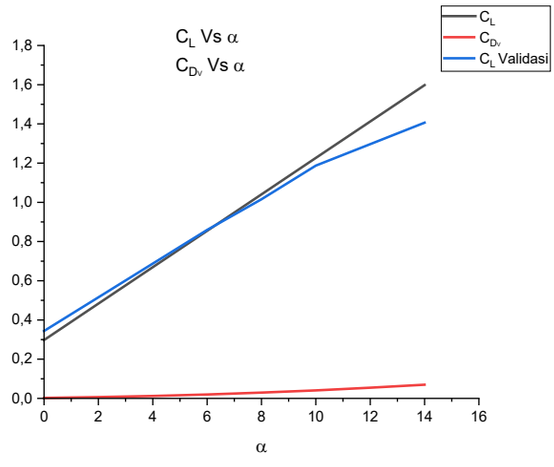

FIGURE 10. C_L vs α and C_{D_v} vs α graph of the 3-D wing validation variant, which is compared with [14].

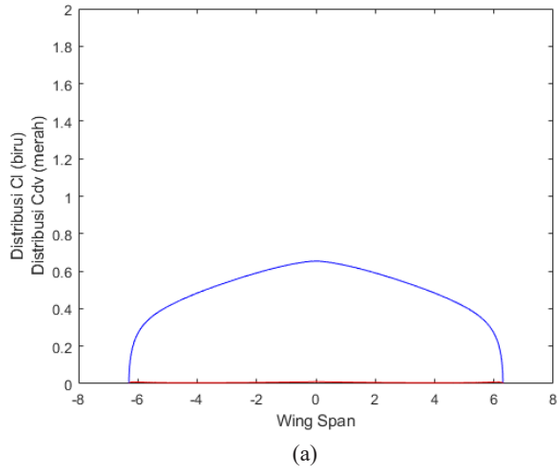

(a)

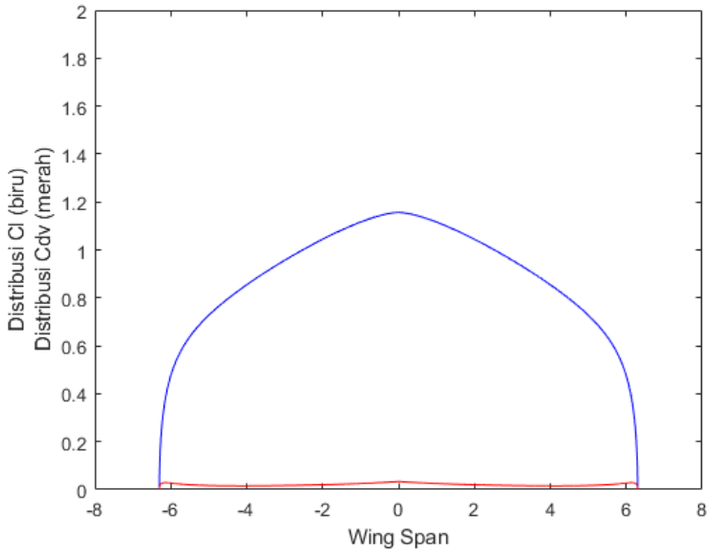

(b)

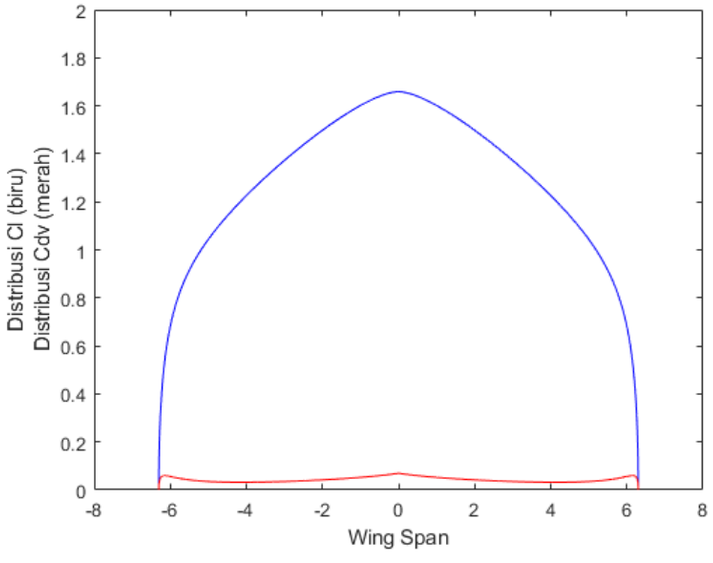

(c)

FIGURE 11. C_l and C_{d_v} distribution along the span of the validation variant with (a) $\alpha = 2^o$, (b) $\alpha = 6^o$, (c) $\alpha = 10^o$.

C_l and C_{d_v} increase as increases. This concur with the theories in (John D. Anderson, 2011) and (Edward Lewis Houghton, 2013). On the other hand, Figure 10 justify the C_L validation with (Justin Petrilli, 2013). Therefore, 8 other variants will be calculated with the same fluid variables and at $0^o \leq \alpha \leq 10^o$. Despite being a potential flow theory, the fluid data, such as Reynolds number and freestream velocity is still needed to obtain the 2-dimensional airfoil data for the calculation of Lifting Line Theory. This is adequate and relevant for subsonic aircraft designs, particularly the commercial ones, since the operating α area of commercial aircrafts are $0^o \leq \alpha \leq 15^o$ (Kermode, 2006) and (Polat, 2018). Same fluids variables are also used for other variants, which are $Re=3\times10^6$ and V=0.2 Mach≈68.6 m/s to obtain the 2D airfoil datas for other variants.

TAPER RATIO VARIANT RESULTS

There are 5 variants that are calculated for the *taper ratio* variant. Variants are specified sequentially from A-TR to E-TR with the smallest λ to the biggest λ (λ=1) with interval of λ =1/6 respectively, as mentioned earlier.

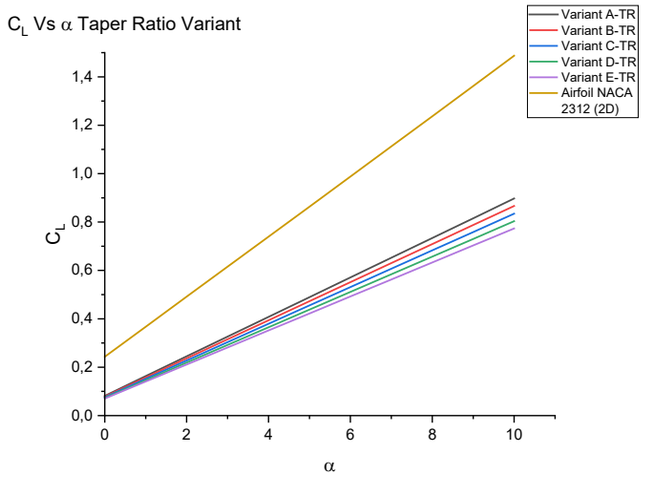

(a)

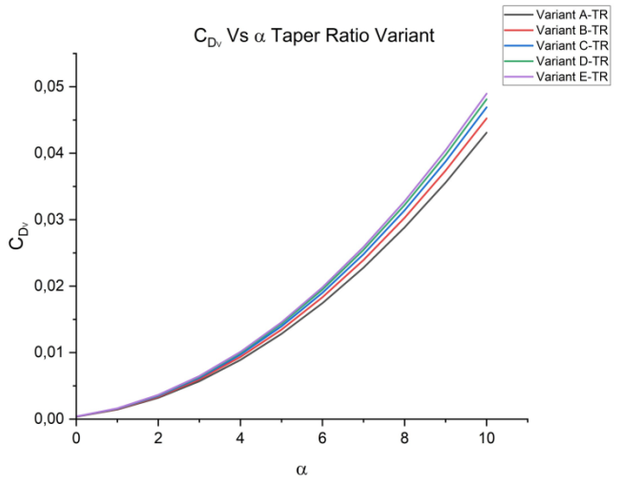

(b)

FIGURE 12. (a) C_L vs α with 2D airfoil data and (b) C_{Dv} vs α graph of the 3-D wing of taper ratio variants.

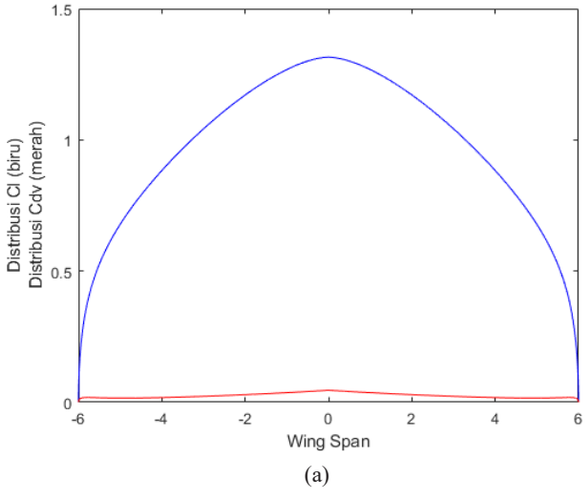

(a)

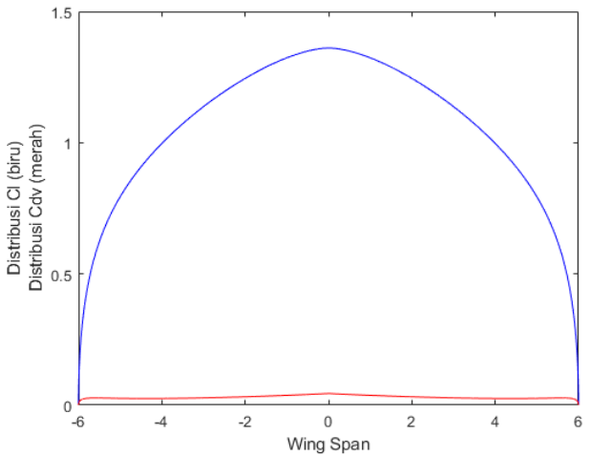
Distribusi Cl (biru)
Distribusi Cdv (merah)
Wing Span
1.5
1
0.5
0
-6
-4
-2
0
2
4
6

(b)

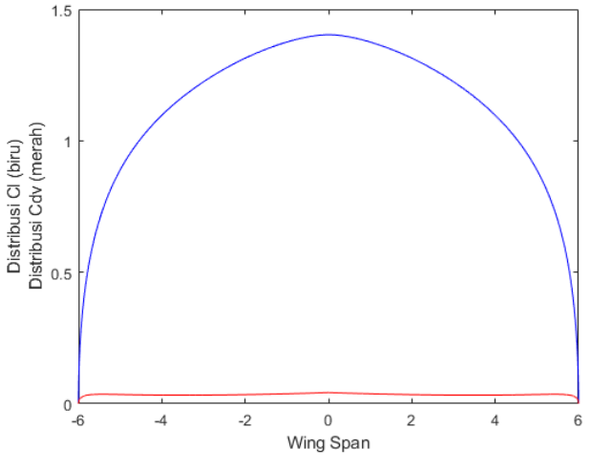
Distribusi Cl (biru)
Distribusi Cdv (merah)
Wing Span
1.5
1
0.5
0
-6
-4
-2
0
2
4
6

(c)

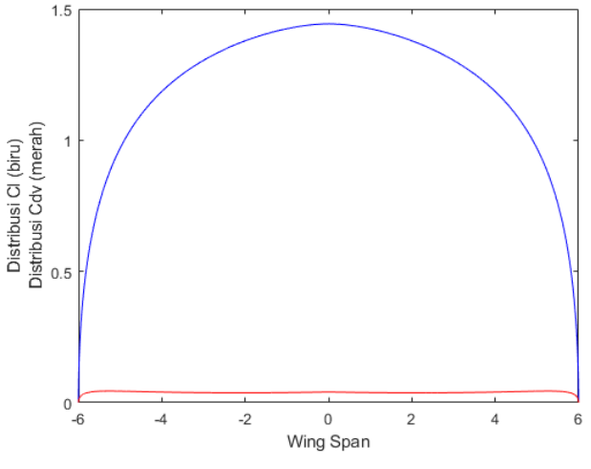
Distribusi Cl (biru)
Distribusi Cdv (merah)
Wing Span
1.5
1
0.5
0
-6
-4
-2
0
2
4
6

(d)

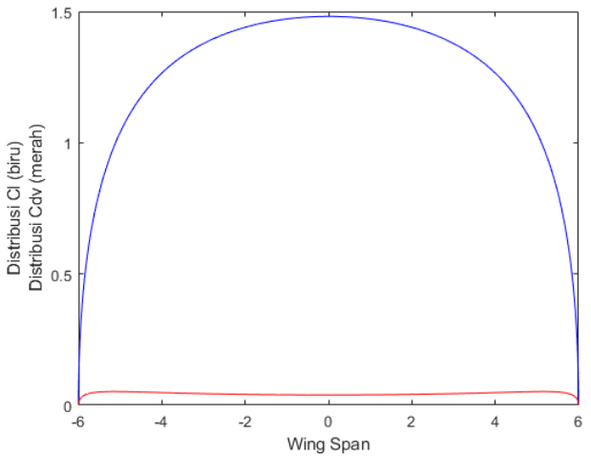

(e)

FIGURE 13. C_l and C_{dv} distribution along the span with α = 5° of the taper ratio variants with (a) A-TR variant , (b) B-TR variant, (c) C-TR variant, (d) D-TR variant, and (e) E-TR variant.

The increase of λ from variant A-TR to E-TR indirectly made the decrease AR of each variant respectively. When λ increases (indirectly decreases AR), C_L of the wing decreases, while C_{D_v} increases, due to affecting the value of both and , as stated in (26) and (30) respectively and can be seen in Figure 12. The C_L decreases by 3% with the increase of λ with 1/6 interval, while C_{D_v} increases by 8.9% with the addition of λ=1/2 at 1/2≤λ≤1 and also increases by 4.4% with the same addition at 1/2≤λ≤1. The distribution of C_l and C_{D_v} is stretched with the increase of , which can be seen in Figure 13. It is also can be seen that the C_L of the 2-dimensional airfoil differs substantially with the C_L of the 3-dimensional with a difference above as can be seen in Figure 12 and Table 1. This is due to the occuring *downwash* that is the consequences of generating lift in a finite wing (John D. Anderson, 2011) and (Edward Lewis Houghton, 2013). Therefore, to obtain suitable perfomance that is desired when designing an aircraft, a good consideration of is required as it affects the ratio of and .

EXPANSION SEGMENT VARIANT RESULTS

This variant utilizes 3 variants to analyze the effect of adding an expansion segment, which will increase C_L and extend the distribution of C_l without extending the wingspan. Variants are specified sequentially from A-S to C-S with a variant of increasing taper ratio of the expansion segment respectively.

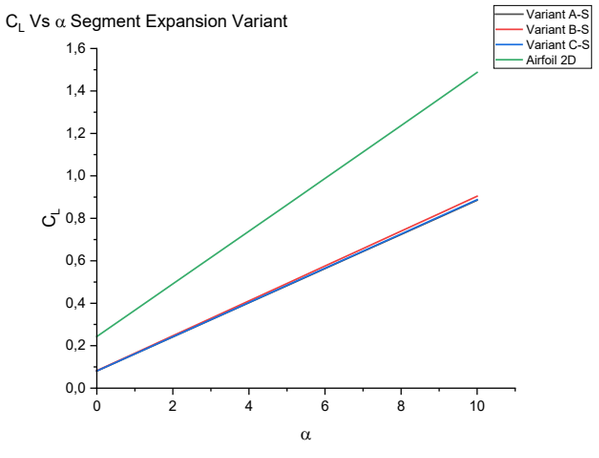

(a)

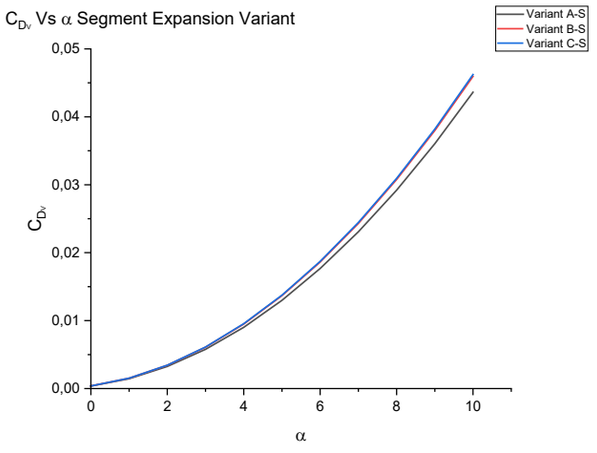

(b)

FIGURE 14. (a) C_L vs α with 2D airfoil data and (b) C_{D_v} vs α graph of the 3-D wing of expansion segment variants.

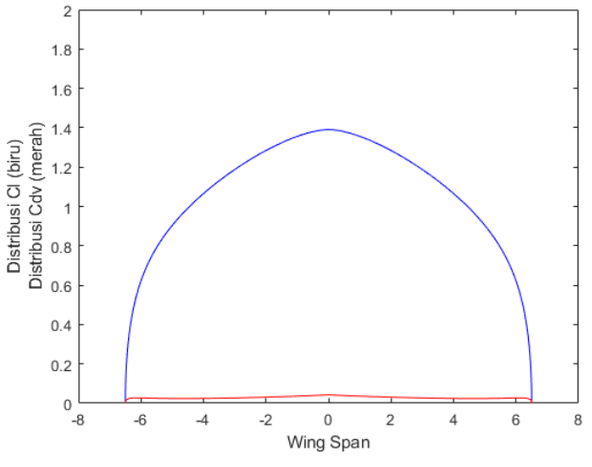

(a)

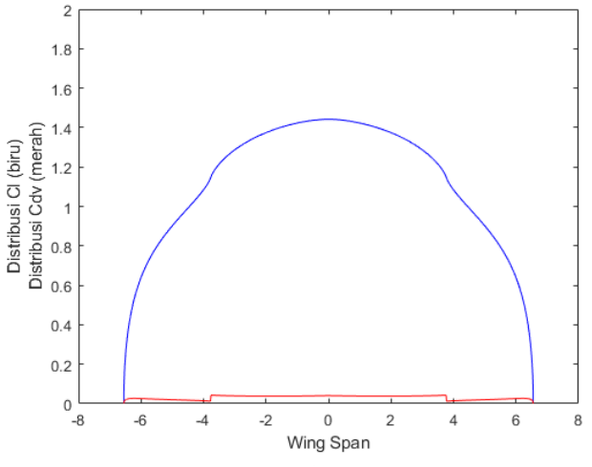

(b)

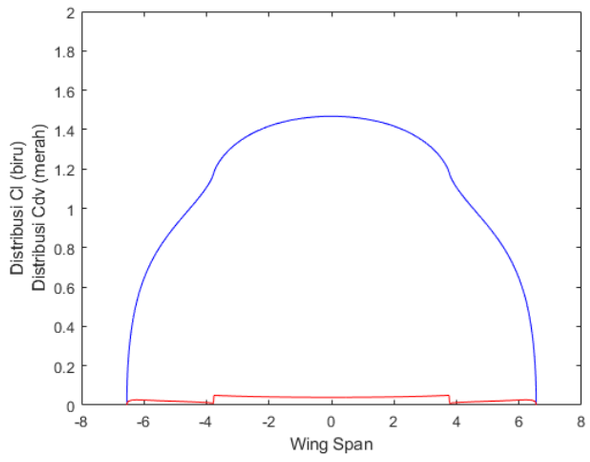

(c)

FIGURE 15. C_l and C_{dv} distribution along the span with α = 5° of the expansion segment variants with (a) A-S variant, (b) B-S variant, (c) C-S variant.

The A-S variant has no expansion segment, while B-S and C-S variant has an expansion segment with increasing λ of the expansion segment, which affects the overall AR of the wing. B-S variant has a higher C_L than the A-S variant, which has no expansion segment. On C-S variant, however, C_L decreases after the increase in B-S variant, despite having a larger expansion segment, which can be seen in Figure 15. The C_{D_v} of both B-S and C-S variant, however, is both larger than the C_{D_v} of A-S variant, which has no expansion segment. This also can be seen in Table 1 that C_L increases by 2.16% from A-S variant to B-S variant and decreases by 0.6% from B-S variant to C-S variant,d espite having larger expansion, as it affects the overall AR of the wing. Meanwhile, the C_{D_v} increases by 5.3% from A-S variant to B-S variant and still increases by 0.6%, despite the decrease of C_L from B-S variant to C-S variant. This justifies the effect of AR to the wing performance as mentioned earlier. Adding an expansion segment to a wing will increase the C_L of and widen the C_l distribution that can be seen in Figure 16. A substantial λ of the expansion segment (λ=1), however, is detrimental to the performance of the wing as it increases C_{D_v} without increasing C_L. Therefore adding an expansion segment to a wing planform shape to increase its performance without adding wingspan is viable, but a good consideration of the λ (recommended λ<1) of the expansion segment and the overall *AR* is required.

PERFORMANCES

To simplify the analysis, differences between C_L and C_{D_v} from all variants is shown in percentage (%) in Table 1.

TABLE 1. C_L and C_{D_v} differences between variants in percentage (%).

Taper Ratio Variant		
A-TR to B-TR	-3.45	5.05
B-TR to C-TR	-3.69	3.67
C-TR to D-TR	-3.74	2.58
D-TR to E-TR	-3.71	1.76
A-TR to C-TR	-7.01	8.90
C-TR to E-TR	-7.31	4.39
C-TR and 2D Airfoil	220.10	-
Expansion Segment Variant		
A-S to B-S	2.16	5.34
B-S to C-S	-1.81	0.59
A-S to C-S	0.31	5.96

The efficiency of a wing, which commonly described by C_L/C_{D_v} ratio (John D. Anderson, 2011) and (Edward Lewis Houghton, 2013), is substituted by C_L/C_{D_v} ratio. TABLE 2 shows the averaged C_L/C_{D_v} ratio of each variant at $0^o \leq \alpha \leq 10^o$.

TABLE 2. Averaged ratio of each variant at

Taper Ratio Variant	Efficiency
A-TR	62.86
B-TR	57.79
C-TR	53.69
D-TR	50.38
E-TR	47.67
Expansion Segment Variant	Efficiency
A-S	61.22
B-S	59.37
C-S	57.95

DISCUSSION

The value of C_L differs substantially from the 2-dimensional airfoil data to the 3-dimensional of the wing due to the downwash that is produced by the consequences of finite wing (John D. Anderson, 2011) and (Edward Lewis Houghton, 2013). The results from Lifting Line Theory do not represent the flow separation that causes stall as presented in (Justin Petrilli, 2013)and is caused by adverse pressure gradient, friction, and viscosity (John D. Anderson, 2011) and (Edward Lewis Houghton, 2013), since it roots from the potential flow theory. This flow separation causes to decrease as can be seen in Figure 10 on . At this condition, no longer increases with . As mentioned earlier, the Reynolds number from the validation was only used to obtain the 2-dimensional airfoil data to run the calculation and was not used otherwise. Lifting Line Theory is still valid as the where the stall condition begins is outside the operating range of most aircraft (take off, cruise, and landing) (Kermode, 2006) and (Polat, 2018), and the stall condition is not considered in aircraft design as aircrafts are not intended to stall.

C_l and c distribution that are shown in Figure 11, Figure 13, and Figure 15 are the sum distribution of various wing condition, albeit affected by fuselage, aileron, or flaps (John D. Anderson, 2011) and (Edward Lewis Houghton, 2013). These conditions are represented with Fourier Series that are included in the calculation with (13). As mentioned earlier, it is justified that the value of AR does affect the C_L and C_{D_v} performance of a wing. Wings with high AR, which have a short C_{tip} shows the decrease of C_l and C_{d_v} distribution as can be seen in previously mentioned figures. This is due to the smaller wing area, which lowers the AR in (32) and affects C_L and C_{D_v} in (26) and (30) respectively. This also shows that increasing wingspan will increases AR and downwash as mentioned in (NASA Editor, 2021). Increasing wingspan has several consequeces that are commonly avoided (Joel F. Halpert, 2010), other methods are used to reduce downwash and C_{d_v} on wingtips, such as adding a geometric twist to the wing (Samuel Merryisha, 2019), or adding a winglet and/or modify the wingtip (Joel F. Halpert, 2010) and (Setyo Hariyadi S.P., 2016).

A common constant to measure a performance of a wing is C_L/C_D ratio (Kermode, 2006) and (Polat, 2018), however, in this article only C_{D_v} is calculated. Therefore, to measure this, we substitute the C_L/C_D ratio with C_L/C_{D_v} ratio. With this constant, wings with substantial AR will perform better than wings with smaller AR as they have higher C_L/C_{D_v} ratio. This can be seen in TABLE 2, where a wing with a high AR (A-TR variant) has an averaged efficiency of 62.86, while wing with small AR (E-TR variant) has an averaged efficiency of 47.67. However, wings with high AR will have more intertia due to the extensive wingspan. This extensive wingspan will also limit the maneuverability of the aircraft and also limit the options for material as high AR wings has extensive wingspan and short airfoil chords (Kermode, 2006) and (Joel F. Halpert, 2010). These craracteristics are suitable for stable, long range aircrafts as they are designed to not move aggresively. Conversely, wings with low AR will have a higher maneuverability and wider options for materials. These characteristics are suitable for fighter and racer aircrafts. In other words, high AR wings sacrifices maneuverabilty to obtain high stability and high C_L/C_{D_v} ratio, while low AR wings sacrifices stability and C_L/C_{D_v} ratio to obtain high maneuverability. On the other hand, while addition of an expansion segment does increase the C_L of the wing, it still decreaes its efficiency as A-S variant

has an efficiency of 61.22, B-S variant has an efficiency of 59.37, and C-S variant has an efficiency of 57.95, which show a decrease. Therefore, C_L and C_{D_v} of a wing planform shape do affect performances of wings, where C_L/C_{D_v} ratio represents the efficiency of a wing and is viable as a measurement to consider when designing an aircraft.

CONCLUSION

Taper ratio value of a wing λ will indirectly affect the aspect ratio *AR* of a wing planform shape. Wings with high λ will have a low *AR* and will cause C_L to decrease and C_{D_v} to increase, and vice versa. On the other hand, adding an expansion segment to a wing will increase C_L significantly. However, C_{D_v} will also increase and higher than the increase of C_L. Because of this, the efficiency of a wing with added expansion segment will decrease nevertheless. To make such addition worthwhile, an acceptable λ of the expansion segment needs to be considered, since an expansion segment with high *AR* will increase only the C_{D_v}. Hence, a good consideration of λ is required in designing aircrafts. To design an aircraft with a fine maneuverability, wings with small *AR* is preferred, and to design an aicraft with a high stability, wings with high AR is preferred. Performance of a wing can also be measured with a ratio of C_L/C_{D_v} a substitute for C_L/C_D. A high C_L/C_{D_v} ratio shows a high efficiency of a wing. However, in aircraft design, a consideration of sacrificing efficiency is required to suit the desired functionality of the aircraft.

ACKNOWLEDGEMENT

This research was supported by Institut Teknologi Sepuluh Nopember Kampus ITS Sukolilo.

DECLARATION OF COMPETING INTEREST

None

REFERENCES

Daniel Floryan, T. V. 2017. Scaling the propulsive performance of heaving and pitching foils. *Journal of Fluid Mechanics 822*.

Edward Lewis Houghton, P. W. 2013. *Aerodynamics for Engineering Students.* 6th ed. Oxford: Elsevier.

Engineering Toolbox. 2003. *U.S. Standard Atmosphere vs Altitude*. Retrieved February 21, 2022, from https://www.engineeringtoolbox.com/standard-atmosphere-d_604.html

Jacob S. Izraelevitz, Q. Z. 2017. State-space adaptation of unsteady lifting line theory: Twisting/flapping wings of finite span. *AIAA Journal*.

Joel F. Halpert, D. H. 2010. Aerodynamic optimization and evaluation of KC-135R winglets, raked wingtips, and a wingspan extension. *48th AIAA Aerospace Sciences Meeting 4-7 January 2010*, 2010-57.

John D. Anderson, J. 2011. *Fundamentals of Aerodynamics* (5th in SI Units ed.). New York: McGraw Hill Education.

Johnson, V. S. 1990. Minimizing life cycle cost for subsonic commercial aircraft. *Journal of Aircraft, 27*(2), 139-145.

Justin Petrilli, N. T. 2013. A CFD database for airfoils and wings at post-stall angles of attack. *31st AIAA Applied Aerodynamics Conference, June 24-27 Fluid Dynamics and Co-located Conferences*, 1-18.

Kazuomi Yamamoto, K. T. 2012. Effect of a nonlinear constitutive relation for turbulence modeling on predicting flow separation at wing-body juncture of transonic commercial aircraft. *30th AIAA Applied Aerodynamics Conference*, 1-14.

Kengo Asada, S. K. 2018. Large-eddy simulation of airfoil flow near stall condition at reynolds number 2.1 x 10^6. *Physics of Fluid* 30.

Kermode, A. C. 2006. *Mechanics of Flight*. 11th edition. (D. R. R. H. Barnard, Ed.) Harlow: Pearson Education Limited.

Luis A. Martinez-Tossas, C. M. 2019. Filetered lifting line theory and application to the actuator line model. *Journal of Fluid Mechanics* 863: 269-292.

Michael D. Bolzon., R. M. 2016. Parametric study of the effects of a tubercle's geometry on wing performance. *AIAA Journal, 54th AIAA Aerospace Sciences Meeting 2016*.

Ming Zhao, M. Z. 2017. Numerical simulation of flow characteristics behind the aerodynamic performances. *Engineering Applications of Computational Fluid Mechanics*.

NASA Editor. 2021. *National Aeronautics and Space Administration*. Retrieved June 29, 2022, from https://www.grc.nasa.gov/www/k-12/airplane/downwash.html

Polat, A. 2018. *Foxnoman*. Retrieved May 19, 2022, from https://foxnomad.com/2018/08/15/how-much-does-the-average-passenger-plane-angle-up-during-take-off/#:~:text=Planes%20slowly%20angle%20up%20during,the%20plane%27s%20tolerances%20of%20course.

Samuel Merryisha, P. R. 2019. Review of winglets on tip vortex, drag, and airfoil geometry. *Journal of Advanced Research in Fluid Mechanics and Thermal Sciences* 63(2): 218-237.

Setyo Hariyadi S.P., W. A. 2016. Numerical study of aerodynamic analysis on wing airfoil NACA 43018 with The addition of forward and rearward wingtip fence. *AIP Conference Proceeding 1778*, 030011-2 to 030011-9.

Slotnick, J. P. 2019. Integrated CFD validation experiments for prediction of turbulent separated flows for subsonic transport aircraft. *NATO Science and Technology Organization Meeting*, (6-1)-(6-14).

Tyler Van Buren, D. F. 2017. Impact of trailing edge shape on the wake and propulsive of pitching panels. *Physical Review Fluids* 2.

Yildirim, B. Y. 2021. Aerodynamic Shape Optimization Of A Wing Using 3D Flow Solutions with SU2 and Response Surface Methodology. Master Thesis, Middle East Technical University, Ankara.

Yunus A. Cengel, J. M. 2014. *Fluid Mechanics, Fundamentals and Applications*. 3rd edition. New York: McGraw-Hill.

Zuhairi A. Rashid, V. B. 2021. Design of aircraft lateral control laws simulation for teaching and learning. *Jurnal Kejuruteraan SI* 4: 117-128.